The cytoskeletal mechanisms of cell–cell junction formation in endothelial cells

Matthew K. Hoelzle and Tatyana Svitkina
Department of Biology, University of Pennsylvania, Philadelphia, PA 19104

ABSTRACT **The actin cytoskeleton and associated proteins play a vital role in cell–cell adhesion. However, the procedure by which cells establish adherens junctions remains unclear. We investigated the dynamics of cell–cell junction formation and the corresponding architecture of the underlying cytoskeleton in cultured human umbilical vein endothelial cells. We show that the initial interaction between cells is mediated by protruding lamellipodia. On their retraction, cells maintain contact through thin bridges formed by filopodia-like protrusions connected by VE-cadherin–rich junctions. Bridges share multiple features with conventional filopodia, such as an internal actin bundle associated with fascin along the length and vasodilator-stimulated phosphoprotein at the tip. It is striking that, unlike conventional filopodia, transformation of actin organization from the lamellipodial network to filopodial bundle during bridge formation occurs in a proximal-to-distal direction and is accompanied by recruitment of fascin in the same direction. Subsequently, bridge bundles recruit nonmuscle myosin II and mature into stress fibers. Myosin II activity is important for bridge formation and accumulation of VE-cadherin in nascent adherens junctions. Our data reveal a mechanism of cell–cell junction formation in endothelial cells using lamellipodia as the initial protrusive contact, subsequently transforming into filopodia-like bridges connected through adherens junctions. Moreover, a novel lamellipodia-to-filopodia transition is used in this context.**

Monitoring Editor
Laurent Blanchoin
CEA Grenoble

Received: Aug 24, 2011
Revised: Nov 1, 2011
Accepted: Nov 9, 2011

INTRODUCTION

Intercellular adhesions are essential for compartmentalization and integrity of tissues in an organism, cell–cell communication, and morphogenesis (Harris and Tepass, 2010). Critical in mediating cell–cell interaction, adherens junctions are formed primarily by cadherin family adhesion receptors and are strengthened by the actin cytoskeleton, which interacts with cadherins through additional proteins. Adherens junctions are especially important for epithelial and endothelial cells that line tissue surfaces and therefore should form cohesive sheets to resist mechanical challenges and maintain tissue integrity.

In epithelial cells, adherens junctions exist in two forms: as stable, linear zonular adherens forming circumferential rings around the apical cell surface in polarized cells, and as dynamic, punctate, discontinuous junctions characteristic for tissues undergoing remodeling or neoplastic transformation (Ayollo *et al.*, 2009; Taguchi *et al.*, 2011). In endothelial cells, the balance between two forms of adherens junctions is shifted toward the dynamic punctate junctions as endothelial sheets must additionally permit solute exchange and especially paracellular transmigration of leukocytes (Harris and Nelson, 2010; Millan *et al.*, 2010). The dynamic nature of endothelial adherens junctions may be further enhanced by inflammatory agents and leukocyte engagement (van Wetering *et al.*, 2002; Bazzoni and Dejana, 2004; Turowski *et al.*, 2008; Dejana *et al.*, 2009; Muller, 2009).

Although a key role of the actin cytoskeleton in the formation and maintenance of adherens junctions is well recognized and molecular linkages between cadherins and actin filaments are largely deciphered (Harris and Nelson, 2010; Harris and Tepass, 2010; Yonemura, 2011), structural organization and specific roles of the actin cytoskeleton at adherens junctions remain largely unknown,

This article was published online ahead of print in MBoC in Press (http://www.molbiolcell.org/cgi/doi/10.1091/mbc.E11-08-0719) on November 16, 2011.

Address correspondence to: Tatyana M. Svitkina (svitkina@sas.upenn.edu).

Abbreviations used: HUVEC, human umbilical vein endothelial cell; TEM, transmission electron microscopy; VASP, vasodilator-stimulated phosphoprotein.

especially in endothelial cells and more generally during initial stages of junction formation. Observations of cell–cell contact initiation in various epithelial cells suggest that the initial contact between migrating cells is made through activity of actin-rich protrusions, lamellipodia and filopodia (Mattila and Lappalainen, 2008). Within the lamellipodium, the actin filaments form a branched network with barbed ends facing the leading edge (Svitkina *et al.*, 1997; Svitkina and Borisy, 1999a). Filopodia, often originating from lamellipodia (Svitkina *et al.*, 2003), are thin bundles of long actin filaments also oriented with their barbed ends toward the filopodium tip (Small, 1988).

Studies of cell–cell junction formation in primary keratinocytes suggested that the initial contact commences with interdigitating filopodia that establish a series of point contacts, which subsequently zipper into a continuous cell–cell junction (McNeill *et al.*, 1993; Raich *et al.*, 1999; Martin-Blanco *et al.*, 2000; Vasioukhin *et al.*, 2000; Vasioukhin and Fuchs, 2001). However, how interdigitating filopodia are first formed has not been reported in these studies. In contrast, work from the Nelson laboratory suggested that lamellipodia establish the initial junction without obvious contribution of filopodia, whereas subsequent contact-dependent inhibition of protrusion in both cells contributes to stable contacts (McNeill *et al.*, 1993; Adams and Nelson, 1998). In either model, extensive reorganization of the actin cytoskeleton is required during early stages of adherens junction formation, but specific actin cytoskeleton architecture during these stages is unclear.

Here we used live-cell imaging combined with platinum replica transmission electron microscopy (TEM) to determine actin architecture at different stages of cell–cell junction formation in primary human umbilical vein endothelial cells (HUVECs). We found that intercellular contact is initiated by lamellipodia, followed by formation of interdigitating filopodia-like structures, which we term bridges. Furthermore, the lamellipodia-to-filopodia transition within the context of cell–cell adhesion occurs by an unconventional mechanism in which the filopodial bundle first forms at the lamellipodium rear and propagates toward the cell edge.

RESULTS

Lamellipodia–to–filopodia-like bridge formation is the predominant event in the initial stages of cell–cell junction formation

To analyze the initial phases of cell–cell junction formation, we used phase contrast live-cell imaging of passage 3 to 4 HUVECs plated on collagen-coated dishes and analyzed at subconfluency. Cell–cell contacts in these cultures were invariably initiated by protruding lamellipodia generated by one or both cells (n = 59). Following retraction of the lamellipodia, thin cytoplasmic bridges connecting two cells were revealed at the point of the lamellipodial contact in 75% of collision events (Figure 1, A and D, and Supplemental Movie S1). In the remaining cases, lamellipodia either did not retract during the 10-min period of observation, or, more frequently, cells separated completely upon retraction (Figure 1D, right). In cases in which bridges were formed, cells subsequently resumed protrusion at the site of the bridge or broke the bridge-mediated cell–cell contact with similar frequencies (Figure 1D, left). The lamellipodia retraction could occur synchronously in both contacting cells, resulting in a broad gap between cells crossed by long bridges (Figure 1C). Alternatively, only one of the two colliding cells retracted and formed a bridge terminating on the flat surface of the other cell (Figure 1B). During their formation, bridges often transiently acquired an hourglass shape characterized by a broad proximal base, a narrow stalk, and a widened distal tip possessing a persistent minilamellipodium (Figure 1C). In other cases, minilamellipodia were not obvious, and the bridges morphologically resembled filopodia in a contact with a neighboring cell throughout the process of their formation (Figure 1B).

HUVECs exhibit different modes of contact with adjacent cells

Light microscopy of bridges formed by HUVECs during junction formation does not allow us to clearly demarcate the boundaries of two interacting cells. Therefore we applied platinum replica TEM to unextracted HUVECs with a preserved plasma membrane to characterize various displays of cell–cell contact at high resolution. We were able to clearly define cell edges in different bridge configurations (Figures 1, E–K).

Examples of contacting lamellipodia of two adjacent cells, which likely corresponded to a very early stage of cell–cell interaction or a case of continuous interplay between contacting lamellipodia, revealed that lamellipodia interacted with one cell completely atop the adjacent cell's lamellipodia or formed interlocking configurations (Figure 1, E and F). Many long, thin bridges were formed by filopodia-like protrusions exhibiting extensive lateral contact with similar structures from the adjacent cell (Figure 1, G and H). Alternatively, a filopodium extending from one cell made a tip contact with the body of the adjacent cell (Figure 1I, top and bottom bridges). Some of these latter bridges exhibited an extensive expansion of the filopodial tip at points of contact resembling minilamellipodia, which we observed by time-lapse microscopy (Figure 1I, second from the top bridge, J, and K). It should be noted that minilamellipodia at the tips of filopodia-like structures were only seen in the context of cell–cell contact, whereas filopodia at free edges possessed a narrow, pointed tip.

Intercellular actin architecture reveals structural similarity of bridges to free-edge filopodia

Platinum replica TEM analysis of detergent-extracted HUVECs revealed the actin architecture in the context of cell–cell contacts. The actin network in overlapping lamellipodia of adjacent cells displayed relatively short-branched actin filaments, as in free-edge lamellipodia, but few, if any, preexisting filopodial bundles (Supplemental Figure S1). However, intercellular bridges displayed tight bundles of long actin filaments similar to those in traditional filopodia (Figure 2, A and B). Further extending the similarity with filopodial bundles, bridge bundles splayed apart at the base of the bridge and merged with the proximal actin network (Figure 2, A and B). Although cell boundaries were no longer recognizable after membrane extraction, some bridges displayed two or more similarly organized subbundles, suggesting that they might correspond to bridges formed by laterally interacting filopodia-like protrusions (Figure 2, A and B). However, in other cases the interaction between interdigitating bundles was too tight to demarcate a boundary (Figure 2C). When minilamellipodia were observed at the tips of bridges, they displayed a dendritic actin network typical for lamellipodia, although the shaft of the bridge contained long, parallel actin filaments, similar to conventional filopodia or bridges without minilamellipodia (Figure 2D).

Two major known types of actin bundles—filopodial bundles and stress fibers—are different in the predominant orientation of actin filaments. In contrast to uniform orientation in filopodia, actin filaments in stress fibers display mixed polarity, with the exception of the focal adhesion area, where all filaments are oriented with barbed ends to the membrane (Cramer *et al.*, 1997; Verkhovsky *et al.*, 1997). To determine whether bridge bundles resemble filopodia or stress fibers with respect of actin filament polarity, we decorated actin

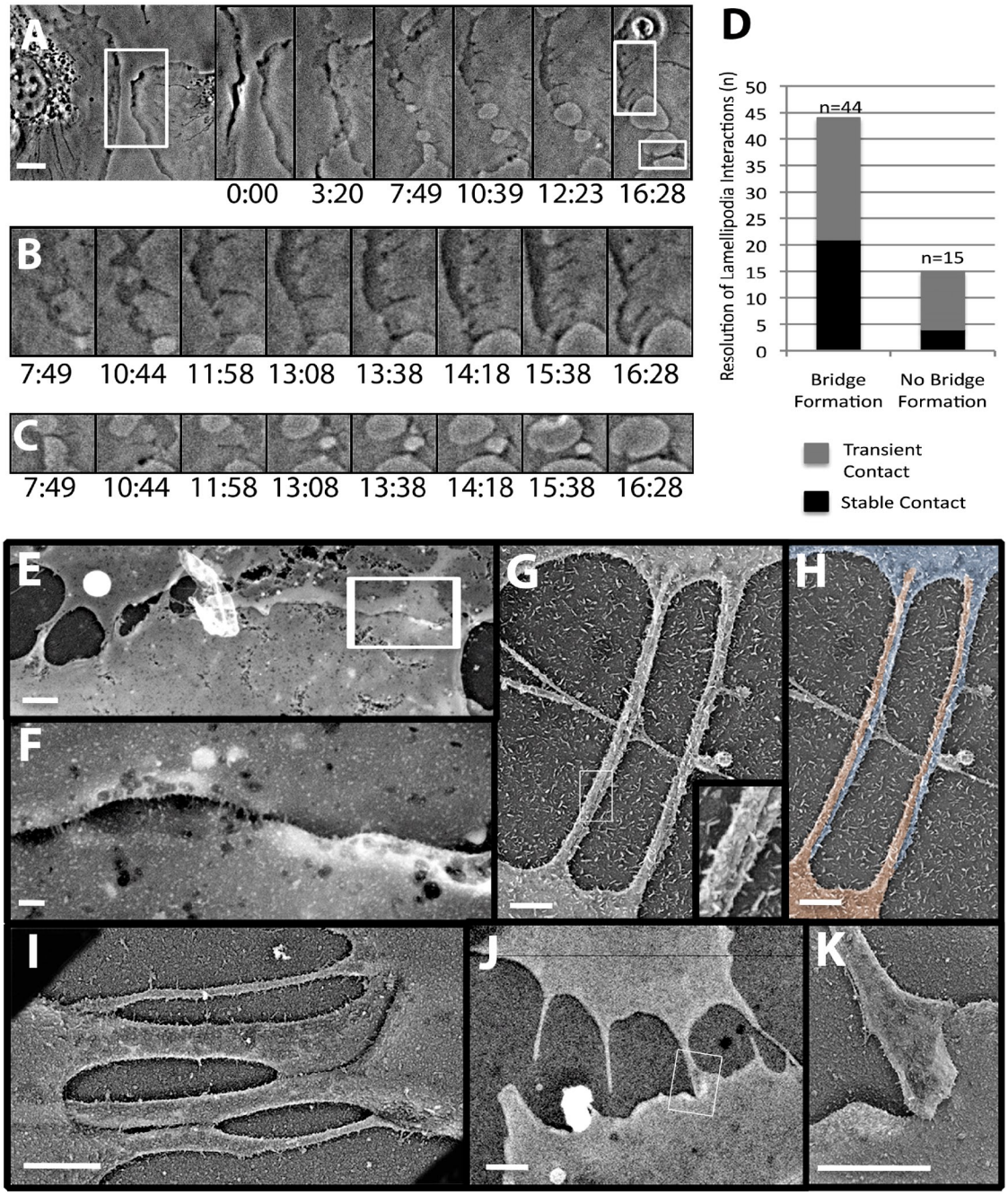

FIGURE 1: The lamellipodia-to-bridge transition during initiation of cell–cell junction in HUVECs. (A–C) Phase contrast time-lapse sequence of junction formation. (A) Left, low-magnification image of two noncontacting cells at time 0. Right, montage of individual frames from the boxed region. Lamellipodia of two cells form initial contact (3:20), followed by lamellipodia retraction and concomitant bridge formation (7:49–16:28). Time in min:s. Boxed regions on the right in A are shown at higher spatial and temporal resolution in B and C. (B) Filopodia-like bridges are formed primarily through retraction of the left cell. (C) Bridges are formed through retraction of both cells with intermediate formation of minilamellipodium (13:08, lower bridge). Scale bar, 15 μm. (D) Quantification of cell–cell collision events (n = 59). Bars show the number of lamellipodia-initiated cell–cell contacts leading to bridge formation (left) or not (right). Gray, transient contacts are broken within 10 min after initiation. Black, stable contacts are defined as greater than 10 min abutting the adjacent cell. (E–K) TEM of unextracted HUVECs showing different types of cell–cell contacts, such as overlapping lamellipodia (E, F), interdigitating filopodia (G, H), or filopodial tips (I) or minilamellipodia (I–K) contacting the surface of adjacent cell. Scale bars, 1 μm (E, J), 500 nm (G–I, K), and 100 nm (F).

filaments in HUVECs with myosin subfragment 1 (S1) and determined filament polarity in contact areas. Myosin S1 decoration revealed that actin filaments in overlapping lamellipodia had barbed ends facing the direction of the leading edge, similar to free leading-edge lamellipodia (Supplemental Figure S2, A and B, respectively). In bridges formed by a single filopodium-like protrusion landing on the surface of the adjacent cell, barbed ends of each filament with detectable polarity were oriented toward the tip of this filopodium, similar to free-edge filopodia (Figure 2E). In bridges that appeared to derive from interdigitating filopodia produced by both contacting

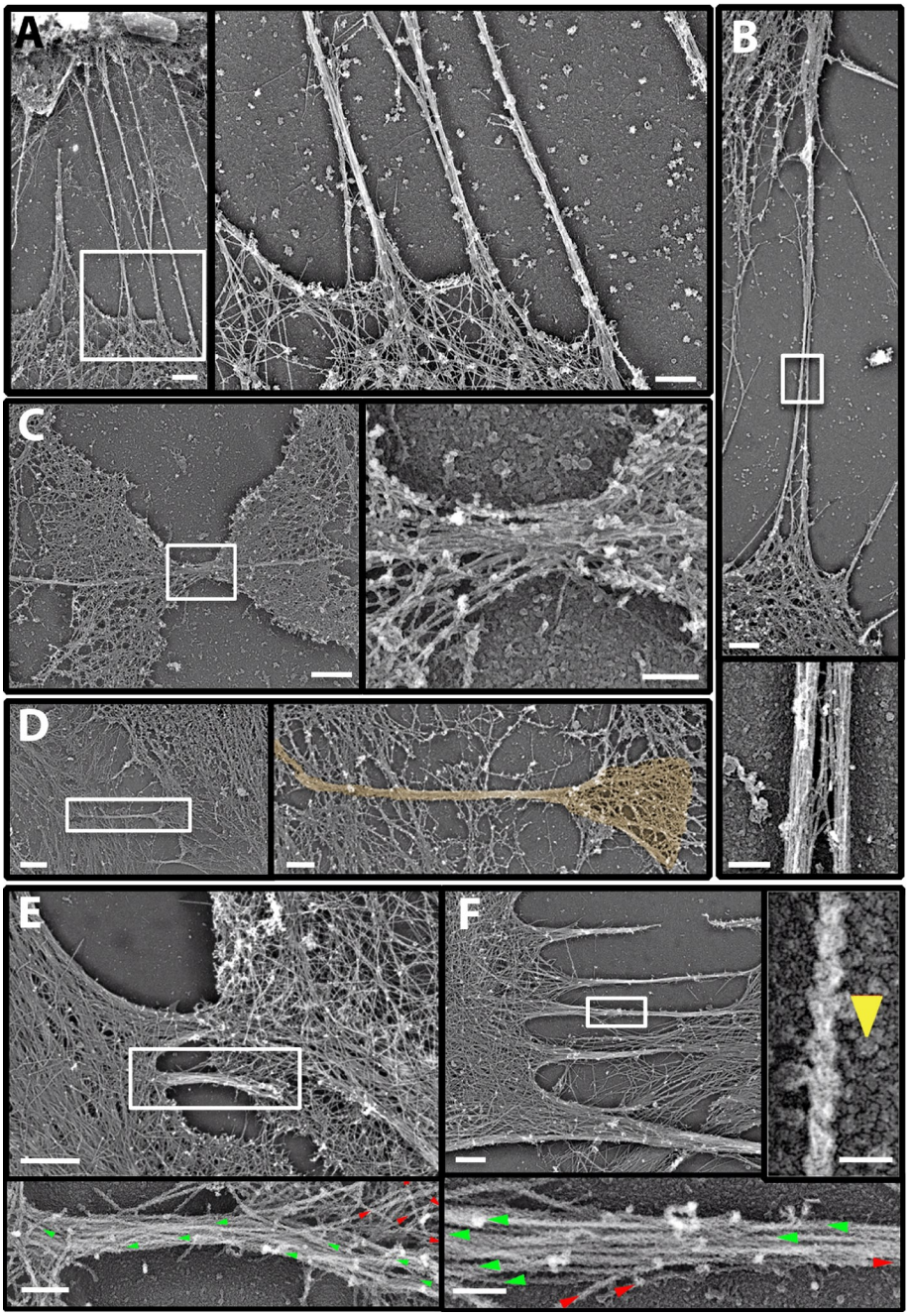

FIGURE 2: Structural organization of actin filaments in intercellular bridges. (A–C) Bridges contact tight bundles of long actin filaments, sometimes splaying apart at the base of the bridge (A, B), similar to free-edge filopodia. Bridges may contain slightly separated subbundles (B) or an apparently single bundle. Boxed regions in main panels are enlarged at right (A, C) or bottom (B). Scale bars, 1 μm (A, B, main), 500 nm (A, zoom; C, main), and 200 nm (B and C, zooms). (D) Minilamellipodia at the tips of bridges (brown) contain a branched actin network, as in free-edge lamellipodia. Boxed region is enlarged at right. Scale bars, 2 μm (main), 500 nm (zoom). (E, F) Myosin S1 decoration of actin filaments within bridges demonstrates barbed-end orientation away from the bridge base in individual (E) and interdigitating (F) bridges. Boxed regions are enlarged at bottom. Arrowheads show direction of pointed ends to left (green) or right (red). Right inset in F shows an individual decorated actin filament with polarity indicated by an arrowhead. Scale bars, 1 μm (E), 500 nm (F), 200 nm (E and F, zooms), and 50 nm (F, inset).

cells, actin filaments at the bases of the bridge were uniformly oriented with barbed ends toward the middle of the bridge, whereas the central region might contain filaments with mixed polarity (Figure 2F), consistent with an idea that the bridge was formed by two filopodia protruding from neighboring cells and forming a junction in the middle of the bridge. Therefore filaments within bridges are similar in both structure and actin polarity to free filopodia.

Bridges contain VE-cadherin and molecular markers of filopodia

To further characterize bridges, we determined their molecular components by immunofluorescence microscopy. VE-cadherin, a key component of adherens junctions in endothelial cells, was highly enriched in bridges, confirming the presence of adherens junctions at sites of bridge formation. VE-cadherin distributions ranged from continuous staining along the shaft of the bridge to single or multiple punctate accumulations (Figure 3A). These findings are similar to previously reported VE-cadherin localization to filopodia-like structures connecting two adjacent endothelial cells (Almagro *et al.*, 2010). In contrast, VE-cadherin antibody stained uniformly and with lower intensity in free (data not shown) or overlapping lamellipodia (Supplemental Figure S3A), suggesting a relocalization of VE-cadherin to bridges upon cell–cell contact initiation. Furthermore, bridges were primarily actin-rich structures with no microtubules present (Supplemental Figure S3B).

Because bridges were similar in structure and filament polarity to traditional filopodia, we tested whether bridges share other key features with filopodia. First, we determined the localization of a bundling protein fascin, which is considered to be a key marker of filopodia (Svitkina *et al.*, 2003; Adams, 2004; Vignjevic *et al.*, 2006; Lee *et al.*, 2010). Consistent with the filopodia-like morphology of bridges, immunostaining of fascin revealed its localization to bridges (Figure 3B).

Next, we performed an actin incorporation assay to examine whether bridges possessed open barbed ends at their tips similar to conventional filopodia. In addition to rhodamine–actin incorporation into free lamellipodia and filopodia in permeabilized cells (Supplemental Figure S3C), open barbed ends were also found in bridges (Figure 3C), suggesting actin bundles within these structures to be actively polymerizing. The sites of rhodamine–actin incorporation were often distributed along a significant distance over the bridge in addition to dot-shaped sites of incorporation, suggesting that open barbed ends might not be always focused at the bridge tip but were distributed along the junction.

Barbed end–associated elongating and anticapping protein vasodilator-stimulated phosphoprotein (VASP) is another conventional filopodial marker, which is enriched at filopodial tips but

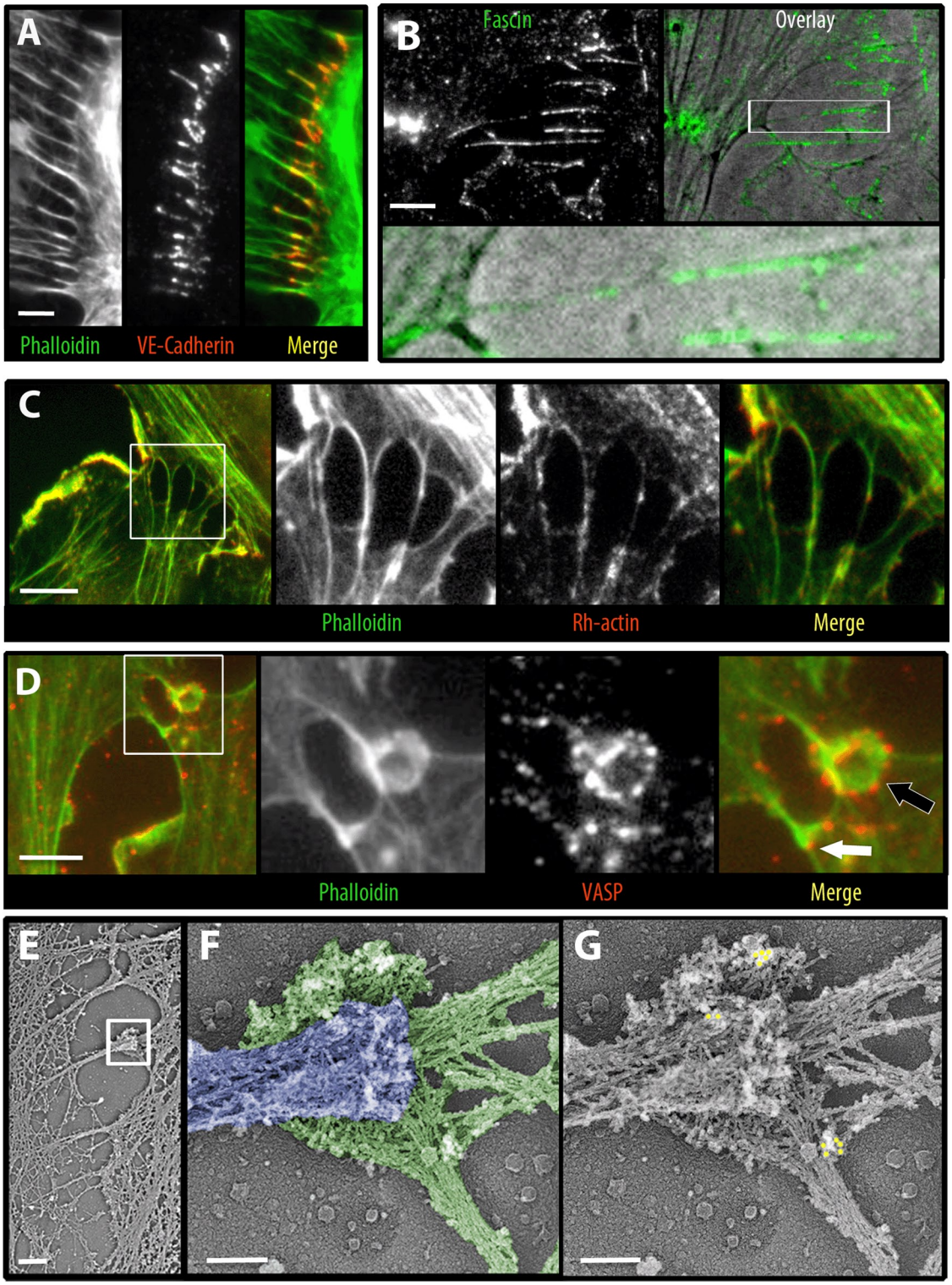

FIGURE 3: Bridges contain adherens junctions and filopodial markers. (A) Immunofluorescence staining of VE-cadherin (red) and F-actin by phalloidin (green). (B) Immunofluorescence staining of fascin shown individually (upper left) and as overlay of phase contrast image (upper right). Boxed region is zoomed at bottom. (C) Actin incorporation assay. Bridges contain uncapped barbed ends incorporating rhodamine-labeled actin (red) into preexisting F-actin structures labeled by phalloidin (green). (D) Left, immunofluorescence attaining of VASP (red) and F-actin staining by phalloidin (green) at low magnification. Right, boxed region zoomed in as individual channels and as a merged image. VASP localizes to bridge tips (white arrow) and along edge of minilamellipodia (black arrow). (E–G) Immunogold staining of VASP. Low-magnification image (E) shows several bridges between interacting cells. Enlarged boxed region from E (F, G) shows structures belonging to two adjacent cells in different colors (F) and position of gold particles (G, yellow). Scale bars, 10 μm (A–D), 1 μm (E), and 200 nm (F, G).

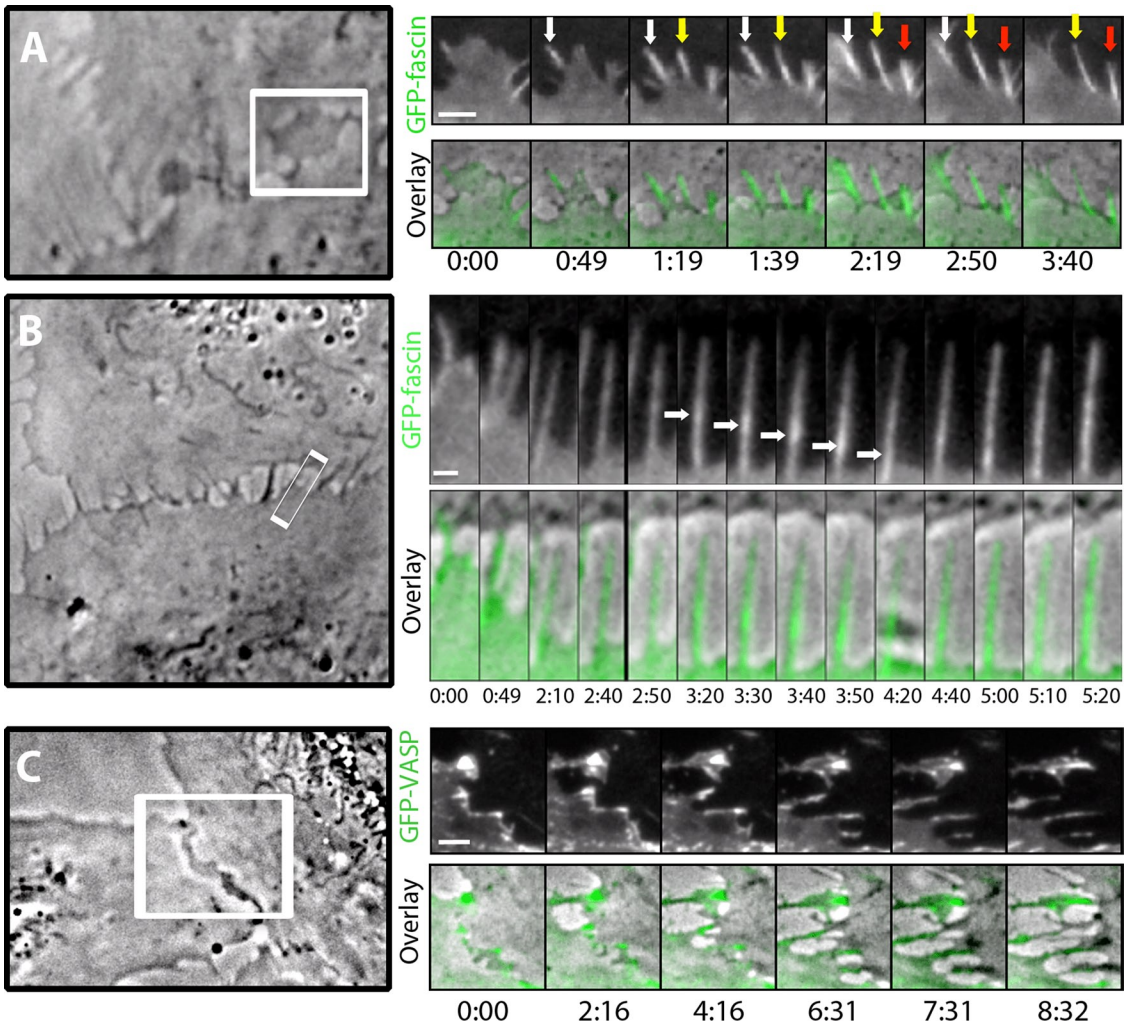

FIGURE 4: Dynamics of filopodial markers in bridges. (A, B) Time-lapse fluorescence microscopy of EGFP-fascin dynamics in nascent (A) and established (B) bridges shown as EGFP fluorescence (upper right) and fluorescence-phase overlay (lower right). Colored arrows in A mark individual protrusions. Arrow in B points to a retrogradely moving feature within the bridge. Left, overviews of the fields. (C) Time-lapse fluorescence microscopy of EGFP-VASP dynamics in nascent bridges shown as EGFP fluorescence (upper right) and fluorescence-phase overlay (lower right). Left, overview of the field. Time in min:s. Scale bars, 10 μm.

also localizes to the leading edge of lamellipodia, cell–matrix adhesions at the tips of stress fibers, and adherens junctions (Krause *et al.*, 2003). Immunostaining of HUVECs with VASP antibody revealed VASP localization at the edge of minilamellipodia and in 68% (n = 25) of bridges (Figure 3D). Immunogold labeling to establish high-resolution localization of VASP by TEM confirmed that VASP localized to lamellipodia edges and free filopodia (Supplemental Figure S4, A and B, respectively), as well as to minilamellipodia and the distal tips of bridges (Figure 3, E–G). A slightly lower fraction of VASP-positive bridges (44%, n = 25) detected by TEM might be due to higher spatial precision of TEM or limited access to dense cytoskeletal regions for gold-labeled antibodies. By both techniques, VASP was usually absent at longer established bridges without minilamellipodia (Supplemental Figure S4C), suggesting a transient requirement of VASP for actin polymerization in bridges or transient elongation of bridges. Together, these data suggest an active branched actin network in minilamellipodia at the tip of bridges, whereas proximal actin bundles at the bridge base, bearing molecular features of filopodia.

Dynamics of molecular markers during bridge formation

During formation of conventional filopodia, fascin is initially recruited to the tip of the filopodial precursor and then propagates along the forming bundle in proximal direction, whereas its steady-state distribution is characterized by highest concentration at the tip and a gradual decrease toward the base of the filopodium (Svitkina *et al.*, 2003). To elucidate the dynamics of fascin during bridge formation, green fluorescent protein (GFP)–fascin transfected HUVECs were analyzed by time-lapse fluorescence microscopy. During cell–cell junction formation, GFP-fascin was not enriched in lamellipodia, but following lamellipodia collapse, it was concentrated in forming bridges (Figure 4A and Supplemental Movie S2). The peak of GFP-fascin enrichment was typically found along the shaft of bridges, whereas the distal and proximal portions of the bridge had dim fluorescence. In hourglass-like protrusions, likely corresponding to minilamellipodia-containing bridges, fascin was enriched at the neck of the protrusion (Figure 4A, 1:39 time point). Owing to uneven distribution of GFP-fascin along the length of the bridge, it was possible to observe persistent movement of individual fluorescent

features in the proximal direction toward the bridge base (Figure 4B and Supplemental Movie S3), suggesting retrograde flow in bridges. Following fascin rearward movement, new regions of GFP-fascin enrichment appeared along the shaft distally but not necessarily at the tip of protrusions, suggesting propagation of the bundle in the distal direction. In contrast to continuous retrograde flow at a fairly constant rate of 2.0 ± 0.4 μm/min, fascin arrival to bridges usually occurred in bursts, when the region of fascin enrichment suddenly expanded in the distal direction by 0.6 ± 0.4 μm (n = 10 bursts, 6 bridges) within one frame of the movie (10 s) with an average interval of 4.3 ± 1.0 min between bursts. In four of 10 bridges GFP-fascin displayed only retrograde flow without bursts of distal expansion.

To investigate the temporal localization of VASP during bridge formation, GFP-VASP transfected primary HUVECs were analyzed with live-cell imaging. In overlapping lamellipodia and in early bridges associated with minilamellipodia, we observed GFP-VASP to enrich at the leading edge of lamellipodia and minilamellipodia (Figure 4C, upper bridge, 0:00 time point, and Supplemental Movie S4). During lamellipodia retraction and bridge formation, GFP-VASP began to condense to distinct puncta or streaks in the forming bridge (Figure 4C, upper bridge, 4:16–7:31). Weak, dot-shaped puncta could be found at the tips of filopodial-like protrusions in bridges, suggesting that they were homologous to VASP at tips of conventional filopodia. In contrast, streaks were more commonly located along the length of the bridge slightly away from the tip, suggesting that they might correspond to the junctional pool of VASP. In mature bridges, dot-shaped tip puncta of GFP-VASP were usually not detectable, whereas streaks persisted over a longer time, suggesting that early filopodia-like bridges might acquire characteristics of junction-associated stress fibers during their maturation.

Bridge formation occurs via a novel lamellipodia-to-filopodia transition

TEM characterization of cell–cell contacts reveals the actin cytoskeleton architecture in detail but does not yield information regarding the temporal sequence in which the initial lamellipodia-like configuration of the cytoskeleton in the protruding edge transforms into filopodia-like bundles in bridges. Therefore we performed correlative TEM to link cell behavior to the high-resolution actin cytoskeletal architecture in HUVECs. Following phase contrast live-cell imaging of cell–cell contact establishment, the same cells were processed for TEM analysis. In the example shown in Figure 5, live-cell imaging (Figure 5A and Supplemental Movie S5) showed that lamellipodia of two initially separated cells came into a contact starting from the upper right corner of the frame (1:15 time point) and expanding toward the lower left (1:15–4:15). After some interplay between two lamellipodia (4:15–5:30), retraction began (6:30) and also progressed from the upper right to the lower left corner of the frame, generating three bridges, among which the top bridge is the oldest, followed by the middle bridge; the lowest bridge is the youngest. Two lower bridges maintained a minilamellipodia at the tip by the time of extraction (7:15), whereas the top bridge did not. Following cell extraction and fixation, TEM investigation of the same region (Figure 5B) showed that the minilamellipodia at the tips of two younger bridges consisted of a branched dendritic network similar to conventional lamellipodia, whereas the bridge shafts contained tight actin filament bundles with seamless transition between two cytoskeletal arrangements (Figure 5, C–E). The oldest bridge in this region contained a typical filopodial bundle without a minilamellipodium at the tip (Figure 5F). Together, our data from correlative light microscopy and TEM showed that bridge formation occurred via collapsing of the lamellipodial actin network into a tight actin bundle starting proximally in the bridge shaft and propagating toward the tip along the entire bridge shaft to form mature bridges containing typical filopodial bundles.

Nonmuscle myosin II gradually invades mature bridges

The formation of bridges concomitantly with the cell edge retraction suggests that cellular contractile forces may contribute to early stages of the process, whereas the distributions of open barbed ends and VASP in mature bridges suggests that bridges may eventually transform into stress fibers. Supporting the latter idea, it has recently been shown that in endothelial cells, actin stress fibers in adjacent cells are linked via adherens junctions (Millan *et al.*, 2010). Our structural TEM data also showed that bridges were sometimes continuous with stress fibers (Supplemental Figure S5). Therefore we investigated the localization and dynamics of nonmuscle myosin II, an indicator of contractile bundles and networks in nonmuscle cells. By immunostaining, although not observed in majority of bridges, there was an accumulation of myosin II in a fraction of bridges, particularly at the bridge base (Figure 6A). High-resolution TEM analysis of the HUVEC cytoskeleton following gelsolin treatment, which dissolves actin filaments while preserving myosin II, showed that when myosin II filaments were present in bridges they were aligned with the bridge axis (Figure 6B-D). To follow the time course of myosin II appearance in bridges, we transfected HUVECs with GFP-tagged myosin light chain (MLC), a subunit of the hexameric myosin II molecule. GFP-MLC localized to stress fibers in a punctate pattern and formed individual puncta in cell lamellae but was absent from lamellipodia. In noncontacting cells and in contacting cells during lamellipodial interplay or beginning of retraction, GFP-MLC puncta in lamellae were found at a significant distance from the leading edge (data not shown). At later time points, myosin II puncta began to accumulate at the bridge base and gradually invaded the shaft of the bridge but did not extend all the way to the tip. In this process, new GFP-MLC puncta appeared distally relative to preexisting puncta, suggesting that myosin II accumulation occurred through de novo assembly of myosin II filaments in bridges similar to the analogous process in the cell lamellae (Svitkina *et al.*, 1997; Svitkina and Borisy, 1999b). Subsequently, the entire array underwent retrograde flow, freeing space for new myosin II puncta (Figure 6, E and F, and Supplemental Movie S6). The rate of myosin II retrograde flow (1.7 ± 0.4 μm/min; n = 12) was not significantly different from the rate of retrograde flow measured in GFP-fascin–expressing cells. Ensuing bridge maturation was characterized by myosin II augmentation at the base and along the shaft, supposedly as the bridge transitions from filopodia-like structure to extension of a stress fiber.

Myosin II activity is essential for bridge formation and VE-cadherin accumulation

Contractile cellular processes are typically driven by myosin II, suggesting a myosin II–dependent mechanism of bridge formation in the course of cell edge retraction. To test this possibility, we examined the effect of blebbistatin, a nonmuscle myosin II inhibitor, on bridge formation. In the control treatment by an inactive (+)-blebbistatin, the lamellipodia-to-bridge transition was the predominant event of initial cell–cell encounter (Figure 7A), similar to untreated cells (Figure 1B). However, when myosin II was inhibited by active (−)-blebbistatin treatment, the frequency of bridge formation was decreased, whereas contacting cells exhibiting sustained lamellipodia interplay with no cellular retraction were the predominant result of initial cell–cell contact (Figure 7A). When bridges did form following collision events in (−)-blebbistatin-treated cells, cells

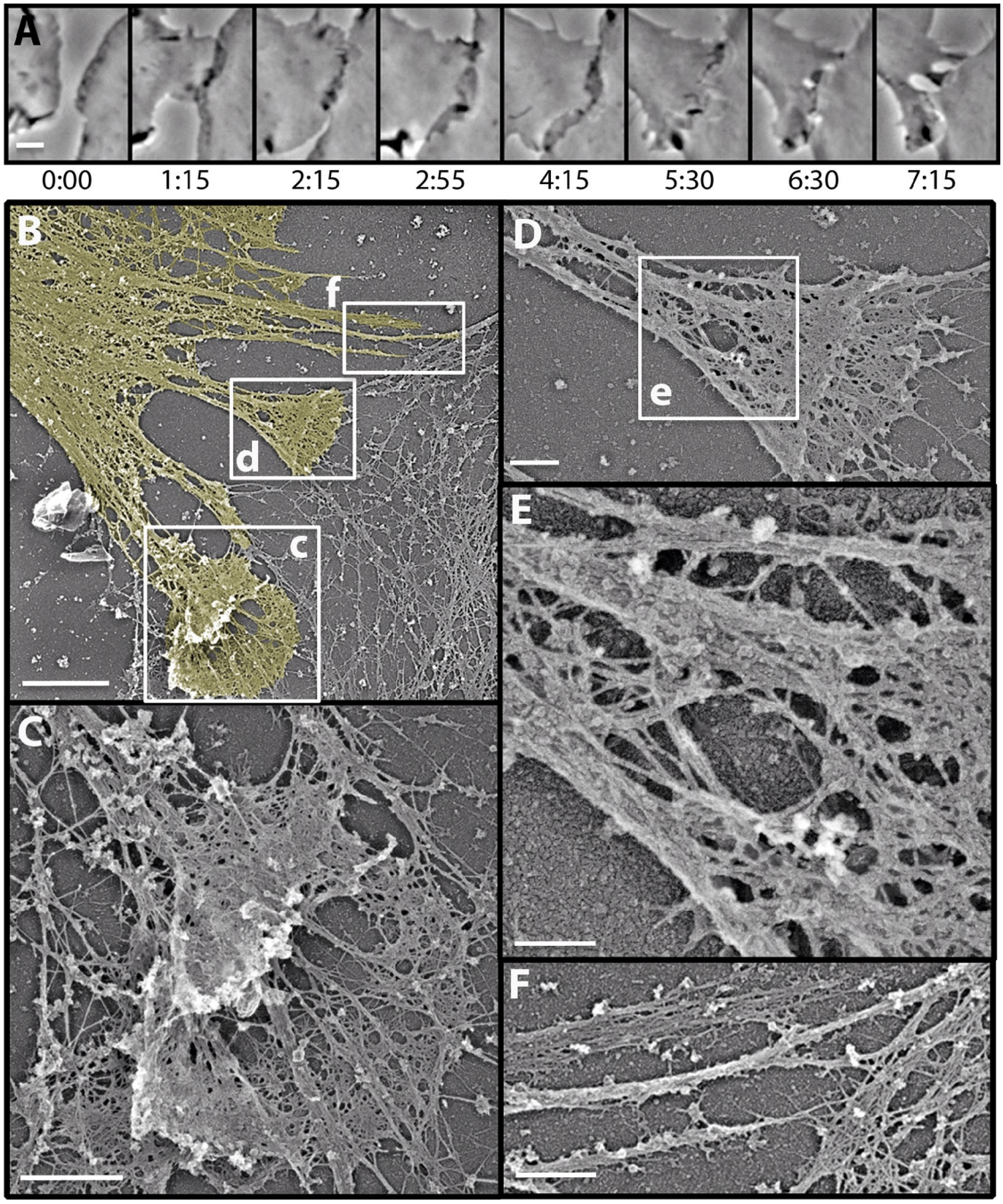

FIGURE 5: Reorganization of the actin cytoskeleton during bridge formation revealed by correlative light and TEM of bridge formation. (A) Phase contrast time-lapse sequence showing following events during formation of nascent bridges: protruding lamellipodia (0:00), initiation of a contact (1:15), expansion of the contact and interplay of lamellipodia (1:15–4:15), beginning of cell edge retraction (5:30), and formation of nascent bridges at the time of extraction and fixation (6:30–7:15). Time in min:s. (B–F) Platinum replica TEM of the same region. (B) Low-magnification image colorized to demarcate cell–cell boundary. Boxes indicate regions magnified in C, D, and F. Actin network in minilamellipodia at the tips of bridges (C, D) gradually transforms into proximally located bundles. Boxed region in D is further magnified in E to show the structure of the transition zone. Mature bridge (F) contains a tight actin bundle without minilamellipodia. Scale bars, 2 μm (A, B), 1 μm (C), 500 nm (D, F), and 200 nm (E).

either resumed protrusion or broke the bridge-mediated cell–cell contact entirely with frequencies similar to those in control samples (Figures 7A and 1B).

Previous studies showed the recruitment of VE-cadherin to established adherens junctions to be stimulated by myosin II–dependent tension force (Liu *et al.*, 2010). To characterize the role of myosin II in VE-cadherin localization during early stages of cell–cell junction formation, immunostaining of VE-cadherin was performed following blebbistatin treatment. VE-cadherin recruitment to cell–cell contacts was dramatically decreased as a result of myosin II inhibition but not entirely abolished (Figure 7B). Quantification of the intensity of VE-cadherin immunostaining demonstrated a drastic decrease of the

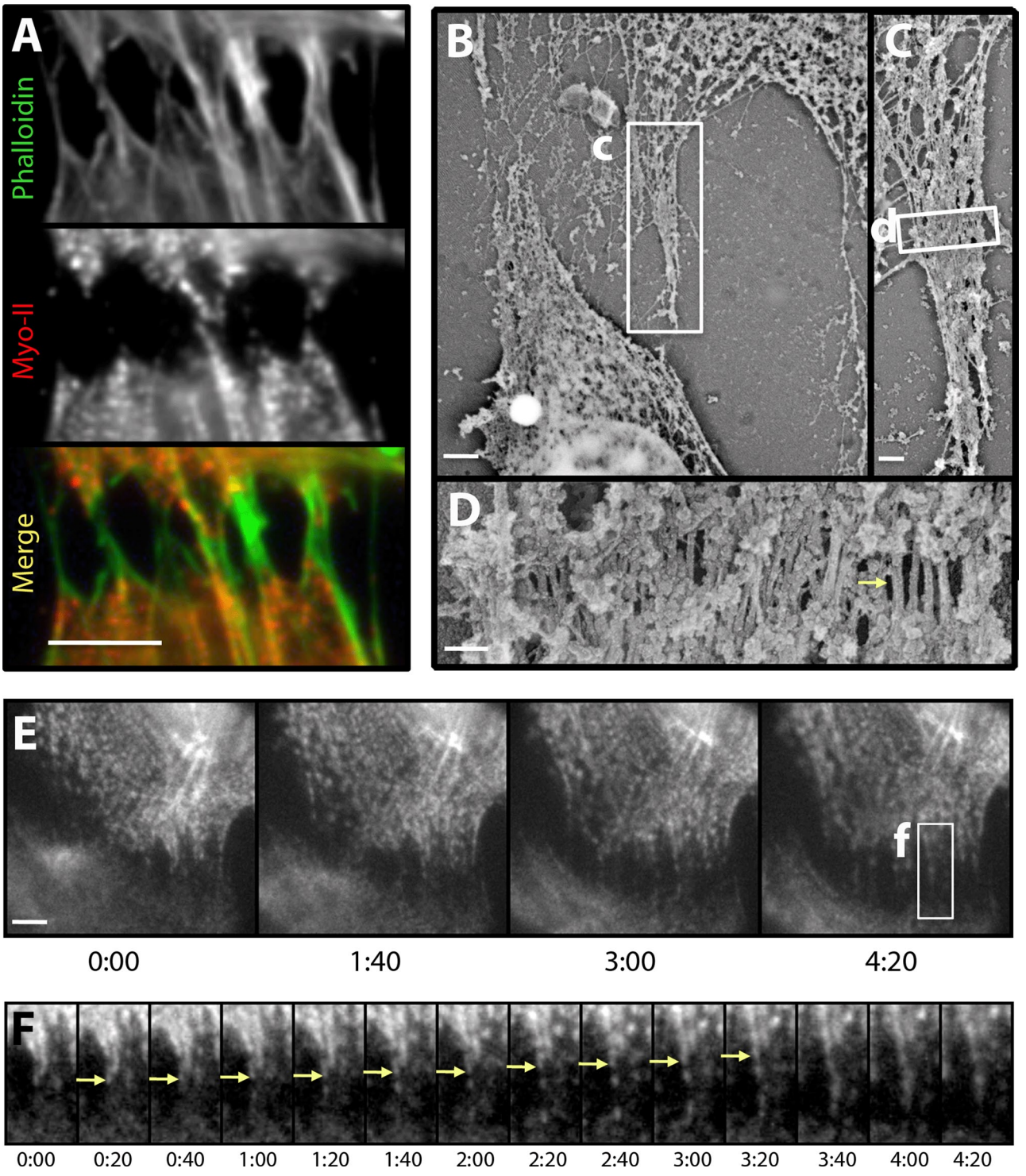

FIGURE 6: Myosin II incorporates into the shaft of mature bridges. (A) Immunofluorescence staining of nonmuscle myosin II (red) and phalloidin staining of F-actin (green) demonstrates presence of myosin II in some bridge bases but not in the bridge shaft. (B–D) TEM of bridges following actin filament removal by gelsolin to expose myosin II filaments. Boxed region in B is magnified in C; boxed region in C is further magnified in D to show a stack of myosin II bipolar filaments oriented along the bridge axis at the base of a major bridge. Myosin II is increasingly absent toward the bridge tip. (E, F) Time-lapse sequence of EGFP-MLC dynamics in intercellular bridges. Boxed region from E is shown at greater spatial and temporal resolution in F. Bright puncta of EGFP-MLC are present in proximal regions of bridges (E); they undergo retrograde flow (arrows in F), while new EGFP-MLC puncta appear distally. Time in min:s. Scale bars, 10 μm (A, E), 2 μm (B), 500 nm (C), 100 nm (D).

total amount of VE-cadherin per bridge after blebbistatin treatment (Figure 7C), whereas the average intensity of VE-cadherin per junction area was only slightly diminished (Figure 7D). These results indicate that myosin II stimulates recruitment of VE-cadherin to nascent junctions, primarily by increasing the size of adherens junctions, with a smaller effect on VE-cadherin density within the junction.

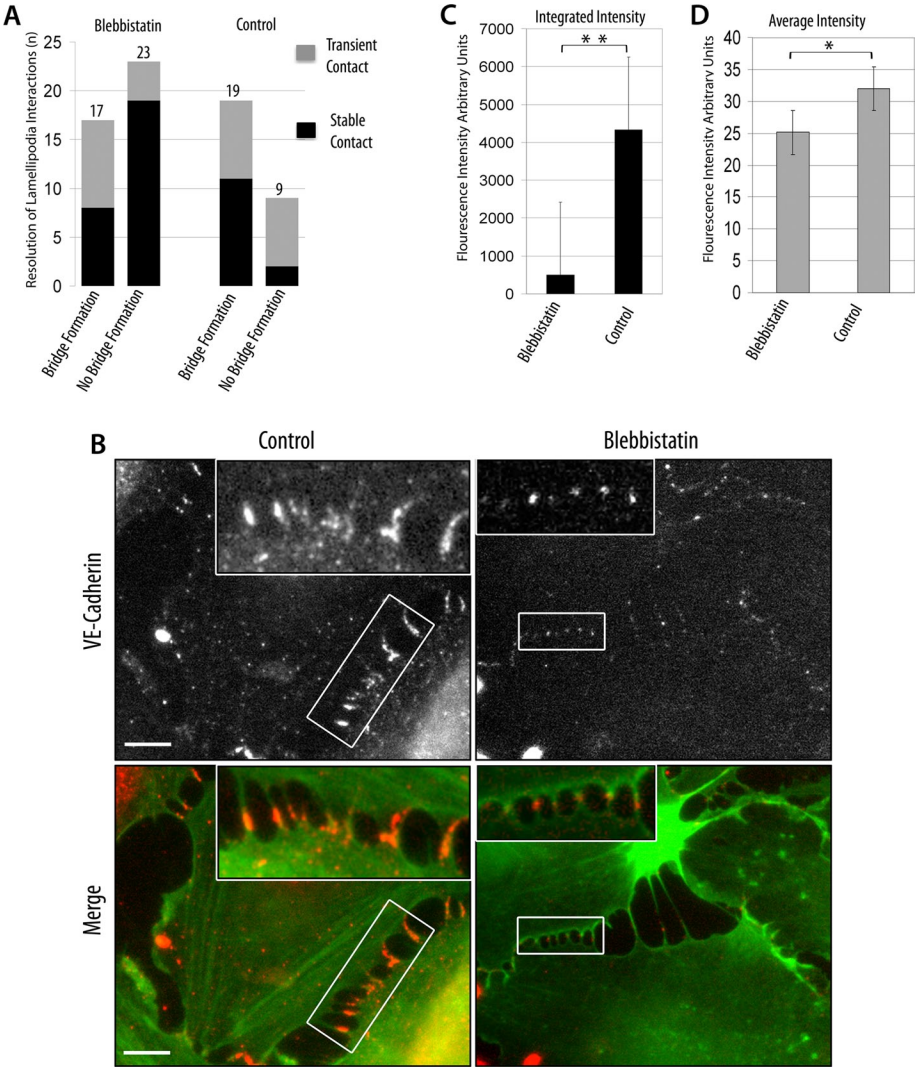

FIGURE 7: Myosin II inhibition results in reduced bridge formation and VE-cadherin accretion. (A) Quantification of cell–cell collision events following treatment with active (−)-blebbistatin (Blebbistatin, n = 40) or inactive (+)-blebbistatin (Control, n = 28). Bars show the number of lamellipodia-initiated cell–cell contacts leading to bridge formation or not. Gray, transient contacts are broken within 10 min after initiation. Black, stable contacts are defined as >10 min abutting the adjacent cell. (B) Immunofluorescence of VE-cadherin (red) and phalloidin staining of F-actin (green) following 30-min treatment with control inactive (+)-blebbistatin (left) or active (−)-blebbistatin (right) reveal reduced size of VE-cadherin puncta following myosin II inhibition. Insets are magnified with equal ratios relative to boxed regions in original image. Scale bar, 10 μm. (C) Quantification of VE-cadherin staining integrated intensity in bridges. Data are represented as mean ± SEM; n = 42 for active (−)-blebbistatin, n = 31 for inactive (+)-blebbistatin. **$p < 0.001$, as determined by a two-sample *t* test. (D) Quantification of VE-cadherin staining average intensity in individual puncta. Data are represented as mean ± SEM; n = 42 for active (−)-blebbistatin, n = 31 for inactive (+)-blebbistatin. *$p < 0.05$ as determined by a two-sample *t* test.

DISCUSSION

In the present study, we show that HUVECs establish initial cell–cell junctions via a previously unknown mechanism using distinct actin-based structures at different stages of the process. We characterize the molecular composition and high-resolution cytoskeletal architecture of these junctional structures and how they transition from one to the other.

First, we determined which protrusive organelles initiate cell–cell junction in endothelial cells. Previously, it was observed that contacts between adjacent epithelial cells are initiated either by lamellipodia, as in MDCK and IAR-2 cells (Krendel and Bonder, 1999; Ehrlich *et al.*, 2002), by filopodia, as in keratinocytes (Vasioukhin *et al.*, 2000), or asymmetrically by lamellipodia of one cell and stress fibers within another cell, as in the CHO cell line (Brevier *et al.*, 2008). In contrast, our data demonstrate that endothelial cells use both types of protrusive structures, but sequentially. Specifically, cell–cell interaction is initiated by lamellipodia of adjacent cells that meet during the protrusive part of their protrusion–retraction cycles, whereas subsequent retraction of lamellipodia leads to the formation of filopodia-like bridges at the points of contact. By applying blebbistatin treatment, we found that the retraction phase is a myosin II–dependent event and that it is required for bridge formation. Incomplete inhibition of cell edge retraction and bridge formation may reflect partial inhibition of myosin II in these conditions. The contractile network of actin and myosin II filaments in the cell lamella is likely responsible for the cell edge retraction and subsequent bridge formation.

We confirmed the identity of bridges as filopodia-like structures based on their cytoskeletal architecture and the presence of conventional filopodial markers—fascin and VASP. The structural and molecular features of bridges and their formation in the course of cell retraction make bridges similar to substrate-attached retraction fibers, which are also filopodia-related structures (Cramer and Mitchison, 1995; Svitkina *et al.*, 2003). Although usually perceived as a byproduct of cell retraction, retraction fibers may in fact represent functional cellular organelles probing the substrate stiffness and adhesion strength, as required for proper cell and tissue morphogenesis (Janmey and Miller, 2011). Filopodia-like bridges may function in analogous capacity during adherens junction formation. In cells exiting mitosis, retraction fibers have been shown to facilitate cell spreading by guiding the extending lamellipodia toward preexisting adhesions (Cramer and Mitchison, 1993; Thery and Bornens, 2006). The respreading of mitotic cells is very similar to the resumed lamellipodial protrusion along intercellular bridges toward nascent bridge junctions, suggesting further functional similarity between bridges and retraction fibers.

The distinct roles of lamellipodia and filopodia in junction initiation revealed here do not necessarily contradict earlier observations (Krendel and Bonder, 1999; Vasioukhin *et al.*, 2000; Ehrlich *et al.*, 2002; Harris and Tepass, 2010) but may instead reflect differences in the mode of junction initiation in endothelial versus epithelial cells. These differences, in fact, seem to extend beyond the junction initiation phase. Indeed, the initial junctional complexes in epithelial cells appear to persistently expand or zipper into a continuous linear junction (Harris and Tepass, 2010), whereas endothelial cells

undergo multiple rounds of bridge formation, followed by resumed lamellipodial protrusion and bridge formation again (Millan *et al.*, 2010). Different dynamic behavior of contacting endothelial and epithelial cells may have functional consequences for relevant tissues. Thus the intercellular gaps in the endothelium transiently provided during spontaneous lamellipodia protrusion–retraction cycles, thereby functionally opening and closing the gate for passage, may be used by leukocytes to exit the blood vessel. Of note, epithelial cells also convert their stable linear junction into more dynamic discontinuous ones during remodeling and migration (Ayollo *et al.*, 2009; Taguchi *et al.*, 2011).

Second, we discovered a novel mechanism of lamellipodia-to-filopodia transformation during bridge formation. Two previous models of filopodia formation were formulated for filopodia emerging from the free leading edge of migrating cells (Yang and Svitkina, 2011). According to the convergent elongation model, free-edge filopodia are initiated from lamellipodia through coalescence of processively elongating lamellipodial filaments that are subsequently bundled by fascin (Svitkina *et al.*, 2003). Nascent filopodia formed by this mechanism are nested within the lamellipodial network at their roots, whereas the actin bundle appears to form in a tip-to-base direction. Another model suggests that a cluster of membrane-associated formins nucleates a filopodial bundle and subsequently maintains their elongation (Steffen *et al.*, 2006; Faix *et al.*, 2009). In contrast to both models, filopodia-like junctional bridges form via the collapse of the lamellipodial actin network into filopodial bundles starting at the base of the lamellipodium and progressing toward the distal tip of the protrusion. Accordingly, accumulation of fascin in bridge bundles progresses not in the tip-to-base direction, as in free-edge filopodia (Svitkina *et al.*, 2003), but in a shaft-to-tip manner. Because fascin is believed to be recruited to preformed parallel bundles (Brill-Karniely *et al.*, 2009; Courson and Rock, 2010), the mode of fascin accumulation in bridges supports an idea of bundle assembly in a proximal-to-distal direction. Of interest, fascin arrival to bridges occurs in discontinuous bursts, suggesting a similar mode of bundle formation. Minilamellipodia persist at the bridge tips as intermediates but disappear as the bridge matures into a tight actin bundle with structural and molecular features of leading-edge filopodia.

The exact origin of long filaments forming the bridge bundle upon lamellipodial collapse remains unclear. However, tight correlation between their appearance and cell retraction suggests force-dependent mechanism(s) of actin cytoskeleton reorganization. One possibility is that the stretch applied to the lamellipodium during retraction promotes debranching and subsequent annealing of short lamellipodial filaments (Skau *et al.*, 2009; Okreglak and Drubin, 2010), which would simultaneously cause loss of lamellipodia and formation of long filaments, as we observed. Another nonexclusive possibility is that a subset of actin filaments in the lamellipodial network undergoes fast, force-assisted elongation, as proposed for formin-associated actin filaments (Kozlov and Bershadsky, 2004), but which may also apply to VASP. Consistent with this idea, open barbed ends in bridges are arranged in the same pattern as VE-cadherin clusters and as VASP streaks formed concomitantly with VASP departure from the lamellipodial leading edge.

Finally, we found that the filopodia-like organization of bridges is a transient state, after which bridges mature into stress-fiber–like structures by incorporating myosin II filaments. Whereas newly formed bridges are devoid of myosin II accumulations, discrete myosin II spots begin to appear in sustained bridges. The mode of myosin II arrival to bridges closely mimics the pattern of myosin II assembly in lamellae (Verkhovsky *et al.*, 1995; Svitkina *et al.*, 1997). In both cases, new myosin II spots are first formed at a distance from the leading edge but in front of preexisting myosin II structures, then undergo retrograde flow, and eventually coalesce with preexisting myosin II accumulations to form actin–myosin II bundles. Subsequently, the mature myosin II–positive bridges likely give rise to fully formed stress fibers associating with adherens junctions in confluent endothelial cells (Millan *et al.*, 2010). Of interest, a similar filopodia-to-stress fiber progression with concurrent accumulation of myosin II was reported for free filopodia in migrating cells (Anderson *et al.*, 2008; Nemethova *et al.*, 2008).

Whereas myosin II has roles in both the construction and deconstruction of F-actin structures (Medeiros *et al.*, 2006; Haviv *et al.*, 2008; Wilson *et al.*, 2010), with respect to cell–matrix adhesions (Chrzanowska-Wodnicka and Burridge, 1996; Bershadsky *et al.*, 2006) or cell–cell junctions (Liu *et al.*, 2010), it is generally believed to mediate force-dependent expansion and stabilization of adhesions. Myosin II also plays a role during initiation of cell–substrate adhesions, although its motor activity is not absolutely required at this stage, and the cross-linking activity is sufficient (Choi *et al.*, 2008). In analogy with these data, we found that myosin II also functions during initiation of cell–cell junctions in the course of bridge formation, although relative contributions of motor and cross-linking activities of myosin II to this process remain to be determined. We suppose that initial cell retraction driven by the contractile actin–myosin II network in the lamella may provide force to induce nascent adherens junctions. When myosin II filaments are subsequently assembled within bridges, they generate greater local force applied to these nascent junctions, leading to junction strengthening and growth. One possible explanation of stimulated assembly of myosin II filaments in bridges is as a result of increased tension there. Indeed, it has been shown that myosin II preferentially accumulates at sites of artificially applied mechanical strain (Fernandez-Gonzalez *et al.*, 2009; Ren *et al.*, 2009). Thus our data suggest a positive feedback mechanism by which the initial VE-cadherin clustering in response to weak retraction-mediated force generates local tension, which promotes further myosin accumulation, subsequently inducing increased VE-cadherin clustering.

On the basis of our data, we propose a model of cell–cell junction formation in endothelial cells (Figure 8) according to which cell–cell interaction is initiated via contact of protruding lamellipodia of adjacent cells. Following cell edge retraction, lamellipodia begin to collapse starting from the rear, which produces an hourglass-shaped bridge with a minilamellipodium at the tip. Whereas the minilamellipodium still contains a branched actin network typical for lamellipodia, the shaft of the bridge contains a filopodium-like actin bundle. At the next stage of the process, the continuing collapse of the lamellipodial network from the rear leads to elongation of the shaft bundle toward the bridge's distal tip. Bundle formation is accompanied by progressive accumulation of fascin, redistribution of VASP from the lamellipodial leading edge toward the bundle tip, and incorporation of myosin II into the bridge base at the later stages of the process. We propose that there is a positive functional relationship between initial point contacts made by lamellipodia and the initiation of bridges at these sites, whereas induced bridges may strengthen the nascent junction and maintain the cells close to each other, which would increase the chances of junction expansion.

Our study gives new insight into the dynamics and architecture of the actin cytoskeleton during cell–cell junction formation in endothelial cells, which will help to more clearly understand how endothelial cells control permeability essential for nutrient flow during embryonic development, as well as in biological phenomena such as leukocyte transmigration.

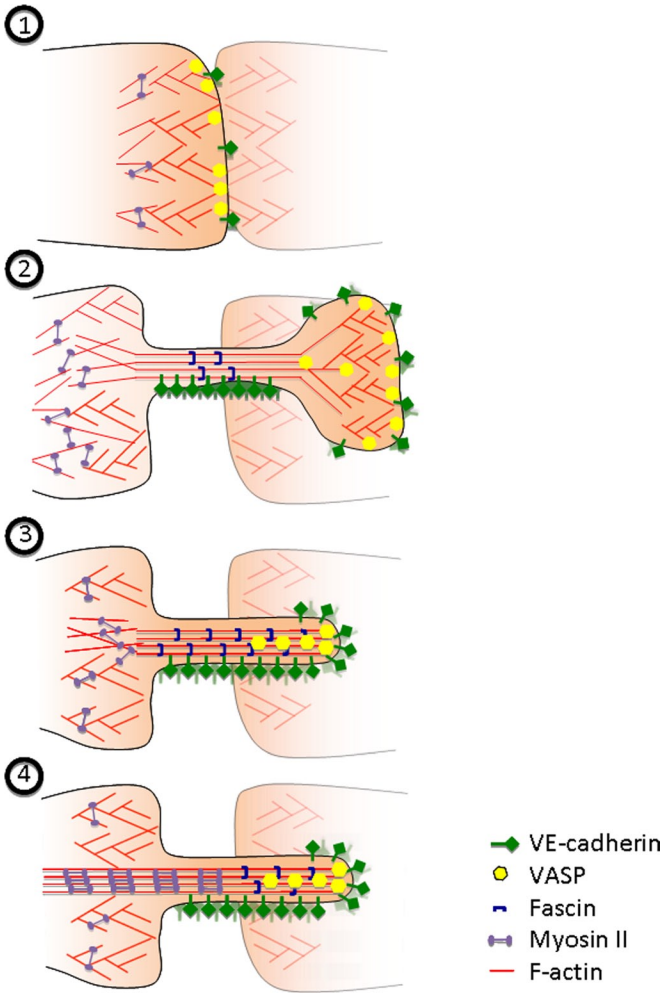

FIGURE 8: Model of cell–cell adhesion formation in endothelial cells. Stage 1, initial cell–cell collision is mediated by protruding lamellipodia containing a branched actin network and using typical lamellipodial proteins, including VASP at the leading edge. Stage 2, cell retraction promotes VE-cadherin clustering and adherens junction formation. Lamellipodia begin to collapse from the rear, forming a nascent bridge. Actin filaments are bundled by fascin in the bridge shaft, while an active lamellipodial network remains at the distal tip in minilamellipodium. Stage 3, minilamellipodial actin network completely collapses. Fascin is progressively recruited to the distal region of the bridge and undergoes retrograde flow with the actin bundle. VASP redistributes from the edge of the minilamellipodium to the tip of the bridge bundle. Myosin II enters the bridge base. Stage 4, myosin II filaments continuously assemble within the bridge and undergo retrograde flow with the bridge bundles. Accumulating myosin II displaces fascin from the bridge and gradually transforms the bridge into a stress fiber.

MATERIALS AND METHODS

Cells and reagents

HUVECs (Lonza, Basel, Switzerland) were maintained in Endothelial Cell Basal Medium supplemented with recommended reagents (Lonza) and cultured for six passages maximally. For experiments, HUVECs were plated on collagen-coated substrates at collagen concentration ~5 mg/cm^2. Rat-tail collagen was purchased from BD Biosciences (San Diego, CA). The following primary antibodies were used: mouse anti–cadherin-5 monoclonal antibody (1:200; BD Biosciences), rabbit polyclonal antibody to nonmuscle myosin II from bovine spleen (1:10; Verkhovsky *et al.*, 1987), mouse monoclonal anti-fascin (1:100, clone 55K2; Chemicon, Temecula, CA), rabbit anti-VASP (1:500; gift of Frank Gertler, Massachusetts Institute of Technology, Cambridge, MA), mouse monoclonal anti-tubulin (1:200, clone DM1A; Sigma-Aldrich, St. Louis, MO). Secondary fluorescently labeled antibodies were from Molecular Probes (Invitrogen, Carlsbad, CA) or Jackson ImmunoResearch Laboratories (West Grove, PA). Myosin subfragment-1 (S1) was a gift from Y. E. Goldman (University of Pennsylvania, Philadelphia, PA). Rhodamine-labeled actin protein, purified from rabbit skeletal muscle, was purchased from Cytoskeleton (Denver, CO). Active (−)-blebbistatin and inactive (+)-blebbistatin (Toronto Research Chemicals, North York, Canada) were prepared from 10 mM stock in DMSO. For experiments, cells were plated on collagen-coated substrates a day before the experiment, treated with (−)- or (+)-blebbistatin at 50 μM concentrations in culture medium for 30 min, and then processed for live imaging or immunofluorescence.

Plasmids and constructs

Human enhanced green fluorescent protein (EGFP)-VASP was a gift of J. Bear (University of North Carolina, Chapel Hill, NC), EGFP-fascin was a gift of J. Adams (Case Western Reserve University, Cleveland, Ohio), and EGFP-MLC was a gift of T. L. Chew and R. Chisholm (Northwestern University, Evanston, IL). For transfection, HUVECs were subjected to nucleofection (Nucleofector I, Amaxa protocol for HUVECs; Lonza). Approximately 5×10^5 cells per nucleofection reaction with 50–70% transfection efficiency were then plated on collagen-coated dishes with fresh media given 1 d after transfection. Cells were analyzed 2–3 d after initial transfection.

Immunofluorescence

Cells were quickly washed with phosphate-buffered saline (PBS) before extraction or fixation. For VE-cadherin staining, cells were fixed in 4% paraformaldehyde in PBS for 30 min. For nonmuscle myosin II immunostaining, cells were extracted with 1% Triton X-100 in PEM buffer (100 mM 1,4-piperazinediethanesulfonic acid [PIPES]–KOH, pH 6.9, 1 mM $MgCl_2$, and 1 mM ethylene glycol tetraacetic acid [EGTA]) containing 4% polyethelene glycol (PEG; molecular weight 35,000) for 5 min, followed by fixation in 4% paraformaldehyde. Fascin staining was performed after methanol fixation (10 min) without extraction. For VASP staining, cells were treated with a mixture containing 0.1% glutaraldehyde and 0.5% Triton X-100 in PEM buffer and then fixed in 2% glutaraldehyde. The actin incorporation assay (barbed-end assay) was performed as previously described (Lorenz *et al.*, 2004). Briefly, wells were incubated with 0.4 mM rhodamine-actin, 0.25 mM ATP, and 0.1% saponin in P-buffer (10 mM PIPES-KOH, pH 6.9, 138 mM KCl, 4 mM $MgCl_2$, 3 mM EGTA) for 2 min, washed in P-buffer, and fixed in 4% paraformaldehyde. For detection of F-actin, staining with fluorescently labeled phalloidin was performed after fixation during incubation. For quantification of VE-cadherin localization in bridges, integrated and average fluorescence intensities of VE-cadherin immunostaining in individual puncta were measured after background subtraction and thresholding of identically acquired images using MetaMorph imaging software (Molecular Devices, Sunnyvale, CA).

Microscopy

Light microscopy was performed using an inverted microscope (Eclipse TE2000; Nikon, Tokyo, Japan) equipped with Plan Apo 100×/1.3 and Cascade 512B charge-coupled device (CCD) camera (Roper Scientific, Trenton, NJ) driven by MetaMorph imaging

software. For live-cell imaging, cells were plated on collagen-coated, glass-bottomed dishes and kept at 37°C for the duration of the experiment. For phase contrast time-lapse microscopy in the presence of blebbistatin a red filter was inserted into the transmitted light path to prevent photoinactivation and phototoxicity of blebbistatin.

Samples for platinum replica TEM and for correlative light and TEM were processed essentially as described (Svitkina, 2007). Briefly, detergent-extracted samples were fixed with 2% glutaraldehyde, tannic acid, and uranyl acetate, critical point dried, coated with platinum and carbon, and transferred onto TEM grids for observation. Detergent extraction was performed for 5 min at room temperature with 1% Triton X-100 in PEM buffer containing 2% PEG and 2 mM unlabeled phalloidin. For determination of cell surface topography, the extraction step was omitted and cells were directly fixed. For gelsolin treatment, detergent-extracted unfixed cells were incubated with 0.4 μg/ml gelsolin (a gift of A. Weber, University of Pennsylvania) in buffer containing 50 mM 2-(*N*-morpholino)ethanesulfonic acid (pH 6.3), 2 mM $MgCl_2$, 0.1 mM $CaCl_2$, and 2 μM paclitaxel for 10 min at room temperature and fixed with 2% glutaraldehyde. For myosin S1 decoration, detergent-extracted unfixed cells were incubated with 0.25 mg/ml S1 in PEM buffer with 5 mM phalloidin for 30 min at room temperature and fixed with 2% glutaraldehyde. For immunogold VASP staining, cells were treated in the same manner as for immunofluorescence, substituting secondary fluorescent antibodies with 18-nm gold-conjugated antibodies incubated overnight and fixed with 2% glutaraldehyde. Samples were analyzed using JEM 1011 (JEOL, Tokyo, Japan) TEM operated at 100 kV. Images were captured by an ORIUS 835.10W CCD camera (Gatan, Warrendale, PA) and presented in inverted contrast. Identification of gold particles was performed at high magnification after contrast enhancement to distinguish them from other bright objects in the samples.

ACKNOWLEDGMENTS

We are grateful to F. Gertler, Y. E Goldman, J. Bear, J. Adams, T. L. Chew, and R. Chisholm for generous gifts of reagents and C. Simon and B. Keith for permission to use the nucleofection device. This work was supported by National Institute of Health Grants GM 70898 and RR 22482 to T.S.

REFERENCES

Adams CL, Nelson WJ (1998). Cytomechanics of cadherin-mediated cell-cell adhesion. Curr Opin Cell Biol 10, 572–577.

Adams JC (2004). Roles of fascin in cell adhesion and motility. Curr Opin Cell Biol 16, 590–596.

Almagro S *et al.* (2010). The motor protein myosin-X transports VE-cadherin along filopodia to allow the formation of early endothelial cell-cell contacts. Mol Cell Biol 30, 1703–1717.

Anderson TW, Vaughan AN, Cramer LP (2008). Retrograde flow and myosin II activity within the leading cell edge deliver F-actin to the lamella to seed the formation of graded polarity actomyosin II filament bundles in migrating fibroblasts. Mol Biol Cell 19, 5006–5018.

Ayollo DV, Zhitnyak IY, Vasiliev JM, Gloushankova NA (2009). Rearrangements of the actin cytoskeleton and E-cadherin-based adherens junctions caused by neoplastic transformation change cell-cell interactions. PLoS One 4, e8027.

Bazzoni G, Dejana E (2004). Endothelial cell-to-cell junctions: molecular organization and role in vascular homeostasis. Physiol Rev 84, 869–901.

Bershadsky AD, Ballestrem C, Carramusa L, Zilberman Y, Gilquin B, Khochbin S, Alexandrova AY, Verkhovsky AB, Shemesh T, Kozlov MM (2006). Assembly and mechanosensory function of focal adhesions: experiments and models. Eur J Cell Biol 85, 165–173.

Brevier J, Montero D, Svitkina T, Riveline D (2008). The asymmetric self-assembly mechanism of adherens junctions: a cellular push-pull unit. Phys Biol 5, 16005.

Brill-Karniely Y, Ideses Y, Bernheim-Groswasser A, Ben-Shaul A (2009). From branched networks of actin filaments to bundles. Chemphyschem 10, 2818–2827.

Choi CK, Vicente-Manzanares M, Zareno J, Whitmore LA, Mogilner A, Horwitz AR (2008). Actin and alpha-actinin orchestrate the assembly and maturation of nascent adhesions in a myosin II motor-independent manner. Nat Cell Biol 10, 1039–1050.

Chrzanowska-Wodnicka M, Burridge K (1996). Rho-stimulated contractility drives the formation of stress fibers and focal adhesions. J Cell Biol 133, 1403–1415.

Courson DS, Rock RS (2010). Actin cross-link assembly and disassembly mechanics for alpha-actinin and fascin. J Biol Chem 285, 26350–26357.

Cramer L, Mitchison TJ (1993). Moving and stationary actin filaments are involved in spreading of postmitotic PtK2 cells. J Cell Biol 122, 833–843.

Cramer LP, Mitchison TJ (1995). Myosin is involved in postmitotic cell spreading. J Cell Biol 131, 179–189.

Cramer LP, Siebert M, Mitchison TJ (1997). Identification of novel graded polarity actin filament bundles in locomoting heart fibroblasts: implications for the generation of motile force. J Cell Biol 136, 1287–1305.

Dejana E, Tournier-Lasserve E, Weinstein BM (2009). The control of vascular integrity by endothelial cell junctions: molecular basis and pathological implications. Dev Cell 16, 209–221.

Ehrlich JS, Hansen MD, Nelson WJ (2002). Spatio-temporal regulation of Rac1 localization and lamellipodia dynamics during epithelial cell-cell adhesion. Dev Cell 3, 259–270.

Faix J, Breitsprecher D, Stradal TE, Rottner K (2009). Filopodia: complex models for simple rods. Int J Biochem Cell Biol 41, 1656–1664.

Fernandez-Gonzalez R, Simoes Sde M, Roper JC, Eaton S, Zallen JA (2009). Myosin II dynamics are regulated by tension in intercalating cells. Dev Cell 17, 736–743.

Harris ES, Nelson WJ (2010). VE-cadherin: at the front, center, and sides of endothelial cell organization and function. Curr Opin Cell Biol 22, 651–658.

Harris TJ, Tepass U (2010). Adherens junctions: from molecules to morphogenesis. Nat Rev Mol Cell Biol 11, 502–514.

Haviv L, Gillo D, Backouche F, Bernheim-Groswasser A (2008). A cytoskeletal demolition worker: myosin II acts as an actin depolymerization agent. J Mol Biol 375, 325–330.

Janmey PA, Miller RT (2011). Mechanisms of mechanical signaling in development and disease. J Cell Sci 124, 9–18.

Kozlov MM, Bershadsky AD (2004). Processive capping by formin suggests a force-driven mechanism of actin polymerization. J Cell Biol 167, 1011–1017.

Krause M, Dent EW, Bear JE, Loureiro JJ, Gertler FB (2003). Ena/VASP proteins: regulators of the actin cytoskeleton and cell migration. Annu Rev Cell Dev Biol 19, 541–564.

Krendel MF, Bonder EM (1999). Analysis of actin filament bundle dynamics during contact formation in live epithelial cells. Cell Motil Cytoskeleton 43, 296–309.

Lee K, Gallop JL, Rambani K, Kirschner MW (2010). Self-assembly of filopodia-like structures on supported lipid bilayers. Science 329, 1341–1345.

Liu Z, Tan JL, Cohen DM, Yang MT, Sniadecki NJ, Ruiz SA, Nelson CM, Chen CS (2010). Mechanical tugging force regulates the size of cell-cell junctions. Proc Natl Acad Sci USA 107, 9944–9949.

Lorenz M, DesMarais V, Macaluso F, Singer RH, Condeelis J (2004). Measurement of barbed ends, actin polymerization, and motility in live carcinoma cells after growth factor stimulation. Cell Motil Cytoskeleton 57, 207–217.

Martin-Blanco E, Pastor-Pareja JC, Garcia-Bellido A (2000). JNK and decapentaplegic signaling control adhesiveness and cytoskeleton dynamics during thorax closure in *Drosophila*. Proc Natl Acad Sci USA 97, 7888–7893.

Mattila PK, Lappalainen P (2008). Filopodia: molecular architecture and cellular functions. Nat Rev Mol Cell Biol 9, 446–454.

McNeill H, Ryan TA, Smith SJ, Nelson WJ (1993). Spatial and temporal dissection of immediate and early events following cadherin-mediated epithelial cell adhesion. J Cell Biol 120, 1217–1226.

Medeiros NA, Burnette DT, Forscher P (2006). Myosin II functions in actin-bundle turnover in neuronal growth cones. Nat Cell Biol 8, 215–226.
Millan J, Cain RJ, Reglero-Real N, Bigarella C, Marcos-Ramiro B, Fernandez-Martin L, Correas I, Ridley AJ (2010). Adherens junctions connect stress fibres between adjacent endothelial cells. BMC Biol 8, 11.
Muller WA (2009). Mechanisms of leukocyte transendothelial migration. Annu Rev Pathol 6, 323–344.
Nemethova M, Auinger S, Small JV (2008). Building the actin cytoskeleton: filopodia contribute to the construction of contractile bundles in the lamella. J Cell Biol 180, 1233–1244.
Okreglak V, Drubin DG (2010). Loss of Aip1 reveals a role in maintaining the actin monomer pool and an in vivo oligomer assembly pathway. J Cell Biol 188, 769–777.
Raich WB, Agbunag C, Hardin J (1999). Rapid epithelial-sheet sealing in the *Caenorhabditis elegans* embryo requires cadherin-dependent filopodial priming. Curr Biol 9, 1139–1146.
Ren Y, Effler JC, Norstrom M, Luo T, Firtel RA, Iglesias PA, Rock RS, Robinson DN (2009). Mechanosensing through cooperative interactions between myosin II and the actin crosslinker cortexillin I. Curr Biol 19, 1421–1428.
Skau CT, Neidt EM, Kovar DR (2009). Role of tropomyosin in formin-mediated contractile ring assembly in fission yeast. Mol Biol Cell 20, 2160–2173.
Small JV (1988). The actin cytoskeleton. Electron Microsc Rev 1, 155–174.
Steffen A, Faix J, Resch GP, Linkner J, Wehland J, Small JV, Rottner K, Stradal TE (2006). Filopodia formation in the absence of functional WAVE- and Arp2/3-complexes. Mol Biol Cell 17, 2581–2591.
Svitkina T (2007). Electron microscopic analysis of the leading edge in migrating cells. Methods Cell Biol 79, 295–319.
Svitkina TM, Borisy GG (1999a). Arp2/3 complex and actin depolymerizing factor/cofilin in dendritic organization and treadmilling of actin filament array in lamellipodia. J Cell Biol 145, 1009–1026.
Svitkina TM, Borisy GG (1999b). Progress in protrusion: the tell-tale scar. Trends Biochem Sci 24, 432–436.
Svitkina TM, Bulanova EA, Chaga OY, Vignjevic DM, Kojima S, Vasiliev JM, Borisy GG (2003). Mechanism of filopodia initiation by reorganization of a dendritic network. J Cell Biol 160, 409–421.
Svitkina TM, Verkhovsky AB, McQuade KM, Borisy GG (1997). Analysis of the actin-myosin II system in fish epidermal keratocytes: mechanism of cell body translocation. J Cell Biol 139, 397–415.
Taguchi K, Ishiuchi T, Takeichi M (2011). Mechanosensitive EPLIN-dependent remodeling of adherens junctions regulates epithelial reshaping. J Cell Biol 194, 643–656.
Thery M, Bornens M (2006). Cell shape and cell division. Curr Opin Cell Biol 18, 648–657.
Turowski P *et al*. (2008). Phosphorylation of vascular endothelial cadherin controls lymphocyte emigration. J Cell Sci 121, 29–37.
van Wetering S, van Buul JD, Quik S, Mul FP, Anthony EC, ten Klooster JP, Collard JG, Hordijk PL (2002). Reactive oxygen species mediate Rac-induced loss of cell-cell adhesion in primary human endothelial cells. J Cell Sci 115, 1837–1846.
Vasioukhin V, Bauer C, Yin M, Fuchs E (2000). Directed actin polymerization is the driving force for epithelial cell-cell adhesion. Cell 100, 209–219.
Vasioukhin V, Fuchs E (2001). Actin dynamics and cell-cell adhesion in epithelia. Curr Opin Cell Biol 13, 76–84.
Verkhovsky AB, Surgucheva IG, Svitkina TM, Tint IS, Gelfand VI (1987). Organization of stress fibers in cultured fibroblasts after extraction of actin with bovine brain gelsolin-like protein. Exp Cell Res 173, 244–255.
Verkhovsky AB, Svitkina TM, Borisy GG (1995). Myosin II filament assemblies in the active lamella of fibroblasts: their morphogenesis and role in the formation of actin filament bundles. J Cell Biol 131, 989–1002.
Verkhovsky AB, Svitkina TM, Borisy GG (1997). Polarity sorting of actin filaments in cytochalasin-treated fibroblasts. J Cell Sci 110 (Pt 15), 1693–1704.
Vignjevic D, Kojima S, Aratyn Y, Danciu O, Svitkina T, Borisy GG (2006). Role of fascin in filopodial protrusion. J Cell Biol 174, 863–875.
Wilson CA, Tsuchida MA, Allen GM, Barnhart EL, Applegate KT, Yam PT, Ji L, Keren K, Danuser G, Theriot JA (2010). Myosin II contributes to cell-scale actin network treadmilling through network disassembly. Nature 465, 373–377.
Yang C, Svitkina T (2011). Filopodia initiation: focus on the Arp2/3 complex and formins. Cell Adh Migr 5, 402–408.
Yonemura S (2011). Cadherin-actin interactions at adherens junctions. Curr Opin Cell Biol 23, 515–522.